www.MaterialsViews.com

Origin of Improved Optical Quality of Monolayer Molybdenum Disulfide Grown on Hexagonal Boron Nitride Substrate

*Yi Wan, Hui Zhang, Wei Wang, Bowen Sheng, Kun Zhang, Yilun Wang, Qingjun Song, Nannan Mao, Yanping Li, Xinqiang Wang, Jin Zhang, and Lun Dai**

Monolayer molybdenum disulfide (MoS_2), a 2D multivalley semiconductor with remarkable optical and electrical properties, has attracted immense attention since its first discovery. Bulk MoS_2 is a hexagonal-crystal layered structure with a covalently bonded S–Mo–S hexagonal quasi-2D network packed by weak van der Waals force. As its thickness decreases from bulk material to monolayer, MoS_2 transfers from indirect-bandgap to direct-bandgap semiconductor.[1] In general, with a unique 2D structure embracing the high-symmetry valleys[2–4] and a strong photoluminescence (PL) (≈1.85 eV)[5,6] in the visible frequency range, monolayer MoS_2 has much to offer in exploration of novel physics[7,8] and fantastic optoelectronic devices.[9–12]

Chemical vapor deposition (CVD) is an efficient method to grow large-area monolayer MoS_2.[13–15] Generally speaking, the commonly used substrate for monolayer MoS_2 is SiO_2/Si, which has considerable trapping states arising from the SiO_2 layer,[16,17] such as the O-dangling bonds on its surface, and light impurities (e.g., Na and K atoms) inside. The trapping states may result in a doping effect on monolayer MoS_2. The effect of trapping states is especially pronounced in low-dimensional materials. Hexagonal boron nitride (h-BN), an insulating isomorph of graphene,[18] with boron and nitrogen atoms occupying the two nonequivalent sublattices, is relatively inert and expected to be free of charged surface states and dangling bonds. Moreover, h-BN possesses a relatively small lattice mismatch (1.4%)[19] with MoS_2. Therefore, using h-BN as substrate may provide a possibility of observing intrinsic properties of monolayer MoS_2.

So far, only a few works have been reported concerning the synthesis of monolayer MoS_2 on h-BN, where the h-BN flakes were either obtained by low-yield mechanical exfoliation[20,21] or by CVD growth using an ammonia borane precursor,[22] which is chemically active. The photoluminenscence (PL) enhancement from monolayer MoS_2 on h-BN substrates was observed.[21,22] Nevertheless, detailed study on the origin of this phenomenon is lacking.

In this work, we devise a high-yield and simple method to grow monolayer MoS_2 on h-BN flakes. The optical quality of monolayer MoS_2 grown on h-BN improves remarkably compared with that grown on SiO_2/Si. We calculated the PL intensity as function of both the h-BN thickness and the PL wavelength, based on light ray propagation in multilayer structure. Combining the theoretical and experimental analysis, we draw the conclusion that the PL and Raman enhancements of the monolayer MoS_2 on the h-BN originate probably from the relatively weak doping effect from the h-BN substrate rather than the optical interference effect suggested previously.[21] Moreover, experimental results show that the A_{1g} Raman mode exhibits a clear stiffening, whereas the E_{2g} mode exhibits a negligible shift. Besides, the intensity ratio of E_{2g} to A_{1g} is smaller, due to the introduction of h-BN. Our work infers that using h-BN as substrate provides a possibility of investigating the intrinsic property of monolayer MoS_2, such as the novel valley-spin related property.

Monolayer MoS_2 was grown by CVD method in a dual-temperature-zone furnace, using S and MoO_3 powders as the sources. Perylene-3, 4, 9, 20-tetracarboxylic acid tetrapotassium salt (PTAS) solution was used as the seeding promoter.[13,20] Chemically synthesized h-BN flakes were dispersed in aqueous PTAS solution, and then spin-coated on 300 nm SiO_2/Si substrates. Bare SiO_2/Si substrates with the spin-coated seeding promoter were used for control. High-purity Ar gas was used as the carrier gas. Corresponding schematic illustration is shown in **Figure 1**a. The growth temperature programming process is plotted in Figure 1b. The temperatures for S and MoO_3 were elevated from room temperature to 160 and 650 °C, respectively, in 40 min, and controlled steadily for 5 min, followed by a natural cooling-off process.

Y. Wan, H. Zhang, Dr. W. Wang, B. W. Sheng, K. Zhang, Y. L. Wang, Q. J. Song, Dr. Y. P. Li, Prof. X. Q. Wang, Prof. L. Dai
State Key Lab for Mesoscopic Physics and School of Physics
Peking University
Beijing 100871, P. R. China
E-mail: lundai@pku.edu.cn

Y. Wan, B. W. Sheng, Prof. X. Q. Wang, Prof. L. Dai
Collaborative Innovation Center of Quantum Matter
Beijing 100871, P. R. China

N. N. Mao, Prof. J. Zhang
Center for Nanochemistry
Beijing National Laboratory for Molecular Sciences
College of Chemistry and Molecular Engineering
Peking University
Beijing 100871, P. R. China

DOI: 10.1002/smll.201502141

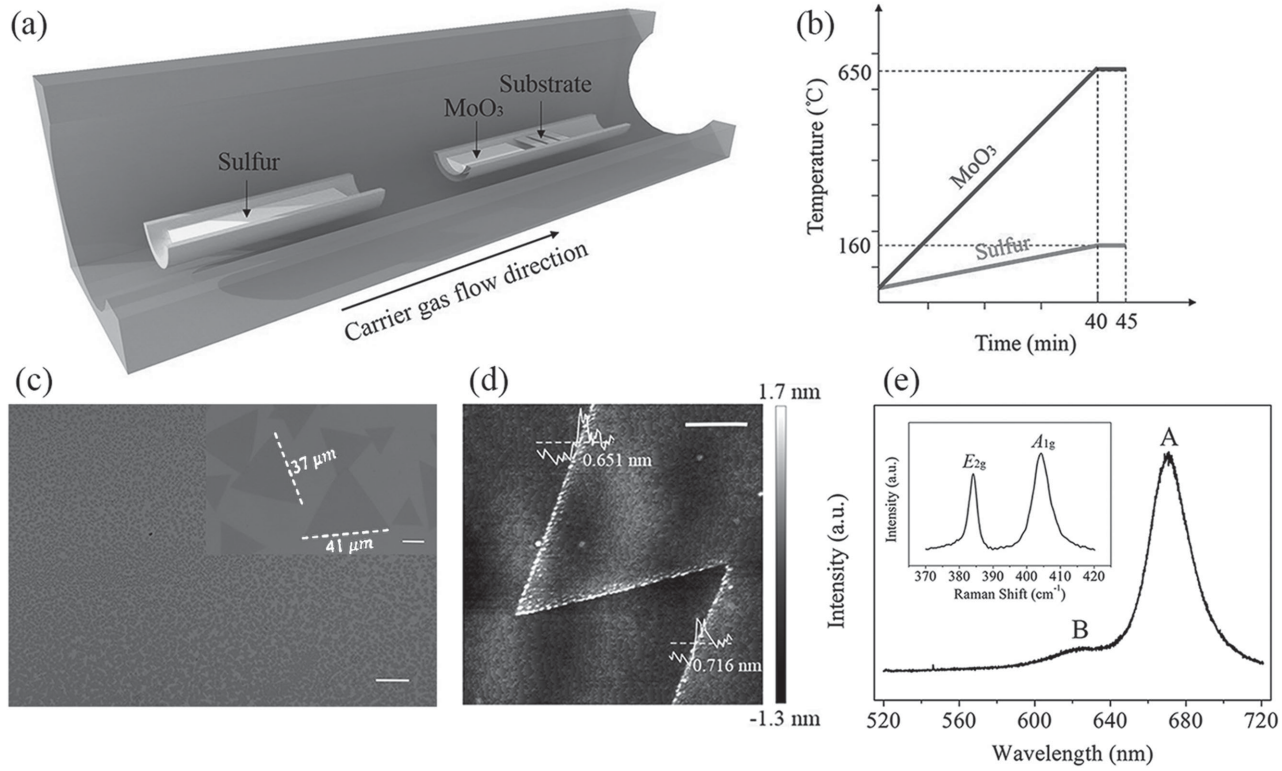

Figure 1. CVD synthesis of monolayer MoS_2 on SiO_2/Si. a) Schematic illustration of the CVD system used for growing monolayer MoS_2. b) The temperature programming process used for a typical growth. c) Optical micrograph of monolayer MoS_2 on a 300 nm SiO_2/Si substrate. The scale bar corresponds to 200 μm. The inset is a zoom-in optical micrograph, where the scale bar corresponds to 10 μm. d) AFM image of monolayer MoS_2, together with the corresponding height analysis. The scale bar corresponds to 1 μm e) Room-temperature PL spectrum from monolayer MoS_2 grown on a 300 nm SiO_2/Si substrate. Inset: the Raman signals from the MoS_2.

Optical micrograph of monolayer MoS_2 grown on a SiO_2/Si control substrate is shown in Figure 1c. Lots of triangle-shaped monolayer MoS_2, which have lateral lengths up to tens of micrometers (see the inset), can be visually distinguished from the substrate due to their obvious difference in the optical contrast.[23–25] The monolayer character of MoS_2 can be further confirmed by the atomic force microscopy (AFM) as shown in Figure 1d, where the thickness of the MoS_2 sample measured along the yellow dashed lines are about 0.651 and 0.716 nm respectively, in consensus with the theoretical value of 0.615 nm for monolayer MoS_2.[26] Figure 1e is the room-temperature PL spectrum of an as-grown monolayer MoS_2. Using excitation of 2.54 eV (488 nm), well above both the two excitonic features, we can clearly see two PL peaks, located at around 1.85 eV (671.6 nm) and 1.98 eV (625.9 nm), respectively. These two peaks result from direct band-edge A- and B-exciton transitions, with the energy split from valence band spin–orbital coupling.[5] The Raman spectrum of it is shown in the inset. We can see clearly the characteristic modes E_{2g} (≈384.0 cm^{-1}) and A_{1g} (≈404.4 cm^{-1}) of MoS_2, which represent the in-plane and out-of-plane atomic vibration,[27] respectively. The peak interval of them is 20.4 cm^{-1}, consistent with the criterion for monolayer MoS_2.[27,28]

An optical micrograph of MoS_2 grown on a 300 nm SiO_2/Si substrate with h-BN flakes on its surface is shown in the inset of **Figure 2**a. Again, we can see lots of triangle-shaped monolayer MoS_2, which have almost merged into a continuous film. The positions, where the h-BN flakes locate, are indicated by orange arrows. Figure 2a is the Raman spectrum measured from the MoS_2 grown on a piece of h-BN flake. We can see the two characteristic peaks of MoS_2, E_{2g} and A_{1g}, as well as the Raman signal from h-BN (≈1366.4 cm^{-1}), confirming that MoS_2 is successfully grown on the h-BN flake.

The PL and Raman spectra of the MoS_2 on an h-BN flake in the orange circle area (labeled as A) are plotted in Figure 2b,c, respectively, together with those of a control sample in the black circle area (labeled as B) for comparison. The PL and Raman spectra of the control sample are quite similar to those shown in Figure 1e, indicating the formation of monolayer MoS_2. Besides, the optical quality of the monolayer MoS_2 has not degraded due to the introduction of the h-BN flakes. One very optimistic finding is that the intensities of both PL and Raman signals from position A are much stronger than their corresponding ones from position B. Noteworthily, there is an observable shift in Raman peak position, especially for A_{1g} mode, which can be seen more clearly in the zoom-in image (Figure S1, Supporting Information).

One of the novel physical properties of monolayer MoS_2 is the valley-spin polarization resolved PL. We also investigated the PL spectrum of monolayer MoS_2 on h-BN under resonant excitation (with the A-exciton) using 633 nm laser, which is commonly used in valley-spin related PL study.[2–4]

www.MaterialsViews.com

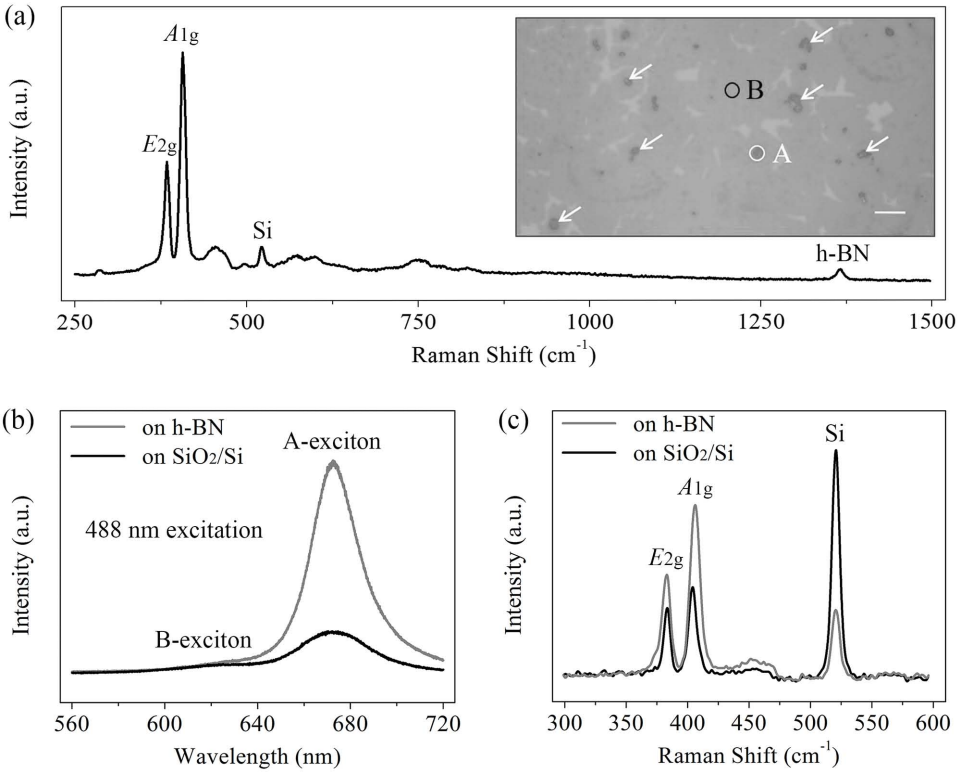

Figure 2. Comparison of optical quality from monolayer MoS_2 on h-BN and SiO_2/Si. a) Raman spectrum of a monolayer MoS_2 on h-BN substrate. Inset: Optical micrograph of the MoS_2 grown on a 300 nm SiO_2/Si substrate with h-BN flakes on its surface. The positions where h-BN flakes locate are indicated by orange arrows. The scale bar corresponds to 10 μm. Two representative samples in the orange and black circles, labeled as A and B, respectively, are adopted for PL and Raman measurements. b) PL and c) Raman spectra of the MoS_2 on the h-BN flake in the orange circle area (see (a)). The PL and Raman spectra of a control sample in the black circle area (see (a)) are also plotted in respective figures for comparison. The excitation wavelength is 488 nm.

Again, we see a clear enhanced PL as shown in **Figure 3**a. This result sheds a light on valley-spin related study. To quantitatively describe the enhanced PL effect of monolayer MoS_2 on the h-BN flake, we define the enhancement factor, $\Gamma = I_A/I_B$, where I_A and I_B are the PL intensities measured at positions of A and B, respectively. The relation of Γ and wavelength is plotted in the inset of Figure 3a, we can see $\Gamma > 1.0$ in the whole wavelength range. Notably, the maximum value of Γ, appearing at A-exciton emission wavelength (≈666.1 nm), is about 5.0. In order to test the universality of these findings, we measured the PL and Raman spectra on dozens of different samples. The PL peak intensities of A-exciton emission from monolayer MoS_2 summarized from 60 samples are plotted in the form of histogram (Figure 3b). Half of the data are obtained from MoS_2 on different h-BN flakes with the thicknesses in a range from 300 to 700 nm (Figure S2, Supporting Information). The other half are obtained from MoS_2 on different h-BN-free positions of substrates with h-BN flakes. The A-exciton emission from monolayer MoS_2 on h-BN flake shows a ubiquitous enhancement compared with that on SiO_2/Si. The detailed correlation between the h-BN thickness and the PL intensity refers to Figure S3b,c in the Supporting Information. The statistical Raman shifts of E_{2g} and A_{1g} modes, together with their intensity ratio, summarized from 40 samples are plotted in the histograms of Figure 3c–e, respectively. At histogram maximum, the Raman shifts of E_{2g} mode measured on both h-BN flake and bare SiO_2/Si are almost equal (≈383.0 cm^{-1}), indicating a negligible shift of E_{2g} mode. However, the Raman shifts of A_{1g} mode at histogram maximum are 406.8 and 404.3 cm^{-1} for monolayer MoS_2 on h-BN flake and on SiO_2/Si, respectively, revealing a stiffening (≈2.5 cm^{-1}) of A_{1g} mode induced by the h-BN substrate. Additionally, we discover that the thickness of the h-BN flakes has negligible influence on the Raman peak position (Figure S3a, Supporting Information). At histogram maximum in Figure 3(e), the values, intensity ratio of E_{2g} to A_{1g}, are 0.55 and 0.75, respectively, for monolayer MoS_2 on h-BN flake and on bare SiO_2/Si substrate. Recent study[29] shows that a decrease in carrier density in monolayer MoS_2 may cause a stiffening of A_{1g} mode as well as a smaller intensity ratio of E_{2g} to A_{1g}.

In order to manifest whether the enhanced PL of monolayer MoS_2 grown on h-BN flake is caused by the optical interference effect in the multilayer structure as suggested in previous work,[21] we calculated the PL intensity as function of both the h-BN thickness and the PL wavelength using the following expression,[21,27,30] which is derived based on light ray propagation in multilayer structure (refer to Figure S4 for detailed derivation process, Supporting Information)

$$I_{MoS_2} = \int_{d_1}^{d_2} \left| F_{exc}(x) \cdot F_{emi}(x) \right|^2 dx \quad (1)$$

where $F_{exc}(x)$ and $F_{emi}(x)$ are the amplitudes for the excitation and emitting light, respectively, and the depth x ranging from d_1 to d_2, represents the ultrathin layer (within the MoS_2 layer)

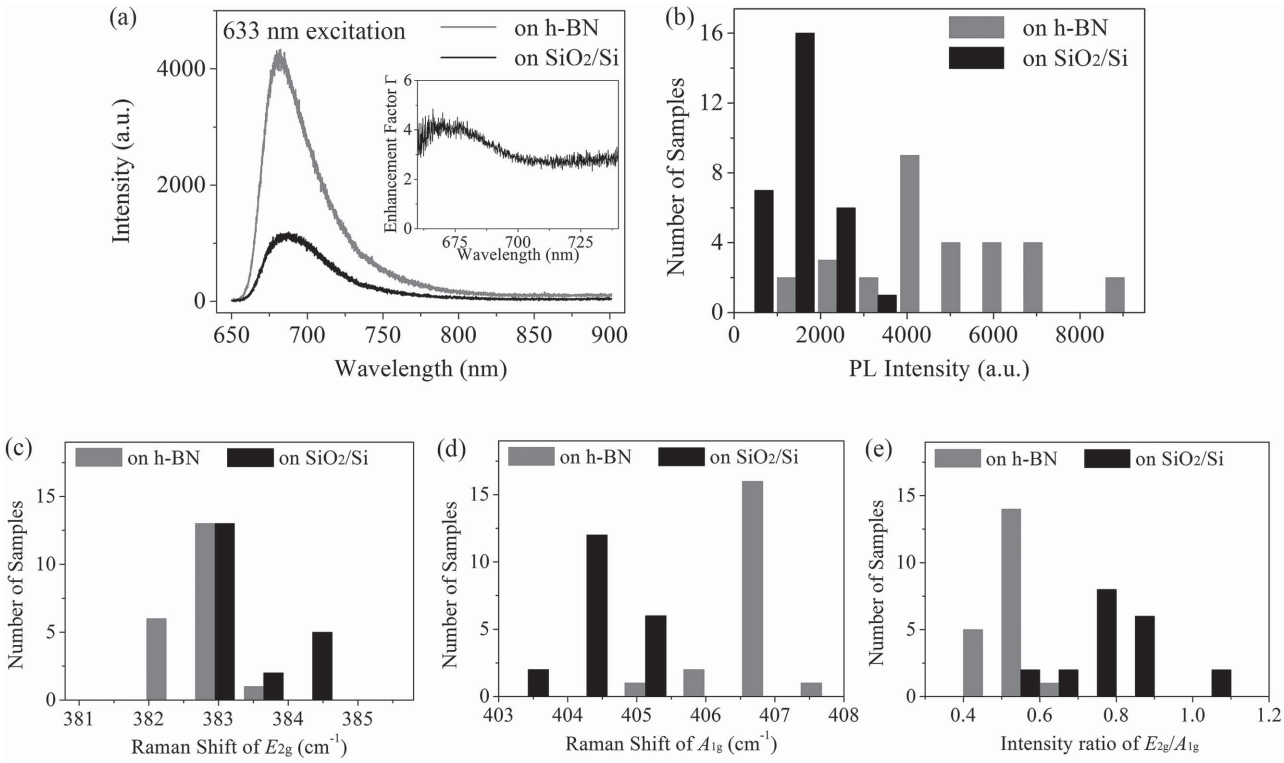

Figure 3. Statistical results of optical measurements. a) PL spectra of the two representative MoS_2 samples on h-BN flake and on 300 nm SiO_2/Si. The excitation wavelength is 633 nm. The inset: the corresponding enhancement factor Γ versus PL wavelength relation. b) Histogram of statistical PL peak intensity measured from monolayer MoS_2 on h-BN (red) and on 300 nm SiO_2/Si (black) summarized from 60 samples. The excitation wavelength is 633 nm. c–e) The histograms of statistical results for Raman shifts of E_{2g} and A_{1g} modes, and their intensity ratio, summarized from 40 samples, respectively. The excitation wavelength is 488 nm.

where the light emitting actually happens. The influence of the depths x for the light emitters on the calculated result has also been discussed (refer to Figure S5, Supporting Information).

Figure 4a is 3D contour plot of the corresponding result normalized by the calculated PL intensity of control sample (namely, the enhancement factor Γ). The refractive index of h-BN is 2.13,[31] and that of monolayer MoS_2 is adopted from our previous work.[32] The 3D curved surface shows the close dependence of Γ on the h-BN thickness. The calculated enhancement factor versus h-BN thickness relation caused by the optical interference at A-exciton emission wavelength (≈671.3 nm) is shown in Figure 4b. Since the A-exciton emission peak position varies slightly for different samples, we choose three representative wavelengths of 666.3, 671.3, and 676.3 nm. The calculated Γ value is less than 1.0 for almost all the thickness range (300–700 nm) of the h-BN flakes used in this work, indicating that the optical interference effect is not only irresponsible for the observed PL enhancement, but

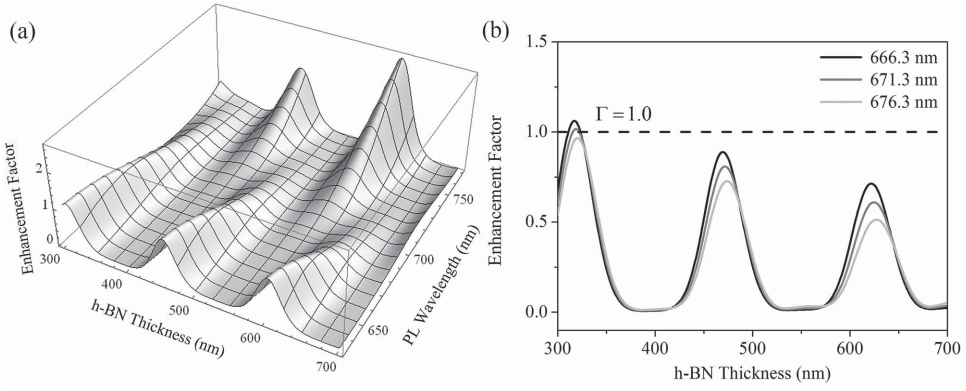

Figure 4. Theoretical calculation upon light ray propagation in a multilayer structure. a) 3D contour plot of the calculated enhancement factor Γ as a function of both h-BN thickness and PL wavelength. b) The variation of Γ (with PL wavelengths of 666.3, 671.3, and 676.3 nm) as h-BN thickness ranging from 300 to 700 nm. The black dashed line corresponds to Γ = 1.0. The integral range used in Equation (1) includes the total thickness of the monolayer MoS_2.

also plays a negative role. Although Γ exceeds 1.0 for some certain h-BN thickness (e.g., 320 nm), it is still much less than the experimental Γ value of around 5.0.

Mak et al. demonstrated that, the PL intensity of monolayer MoS_2 is highly dependent on the electron doping level.[33] When external electrons are introduced, photogenerated electron–hole pairs can be tightly bound by them to form negative quasiparticles, leading to a reduction of PL. Compared with SiO_2/Si substrate, h-BN is relatively inert and expected to be free of charged surface states and dangling bonds, which may induce a relatively weak doping effect on MoS_2. The above Raman measurement result also confirms it. Based on the discussion above, we deduce that it is the relatively weak doping effect of the h-BN substrate on the monolayer MoS_2 that is responsible for its PL and Raman enhancement, rather than the optical interference effect suggested in previous studies.

In conclusion, we have devised and realized a high-yield and convenient method to synthesize monolayer MoS_2 directly on h-BN flakes via the CVD method. Compared with that grown on SiO_2/Si substrate, the monolayer MoS_2 grown on h-BN exhibits enhanced PL and Raman signals as well as the smaller intensity ratio of E_{2g} to A_{1g}. Besides, its A_{1g} Raman mode exhibits clear stiffening, whereas its E_{2g} mode exhibits a negligible shift. We have calculated the PL intensity as function of both the h-BN thickness and the PL wavelength, based on light ray propagation in multilayer structure. Combining the theoretical and experimental analysis, we draw the conclusion that the enhanced PL and Raman signals of monolayer MoS_2 originates probably from the relatively weak doping effect from the h-BN substrate, rather than the optical interference effect suggested previously. Using h-BN as substrate may provide a possibility of investigating the intrinsic property of monolayer MoS_2, such as the novel valley-spin related property.

Experimental Section

Sample Preparation: Uniform and large-area monolayer MoS_2 was grown by a CVD method in a dual temperature zones system, using S (99.999%, Ourchem) and MoO_3 (99.99%, Ourchem) as sources, PTAS as a seeding promoter, high-purity inert argon as carrier gas. During the deposition process, the argon flow rate is 10–20 sccm. Prior to the CVD growth of MoS_2, h-BN flakes (99.5%, XFNANO) were spin-coated on 300 nm SiO_2/Si substrate. Bare 300 nm SiO_2/Si was used as control substrate.

Measurements and Characterization: Optical micrographs were taken by using an optical microscope (Zeiss Axio Imager, A2m). The thickness of monolayer MoS_2 was measured by AFM (Bruker Dimension Icon-PT). PL spectrum was measured by a confocal Raman microscopic system (Horiba, Labram HR800) using a long-working-distance 50× objective. The excitation laser wavelengths were 488 and 633 nm. Raman spectra were recorded by a scanning near-field Raman spectrometer (Witec, Alpha 300RSA) using a long-working-distance 100× objective. The excitation laser wavelength was 488 nm. The Raman signal from Si (≈520.7 cm^{-1}) was used for wavenumber calibration during the Raman measurement. The size of the focused light beam was less than 2 μm. To avoid edge or corner effect, only h-BN flakes close to or larger than 2 μm were used in measurements. All measurements were performed at room temperature.

Supporting Information

Supporting Information is available from the Wiley Online Library or from the author.

Acknowledgements

This work was supported by the National Basic Research Program of China (Grant Nos. 2013CB921901 and 2012CB932703) and the National Natural Science Foundation of China (Grant Nos. 61125402, 51172004, 11474007, and 61404003).

[1] K. F. Mak, C. Lee, J. Hone, J. Shan, T. F. Heinz, *Phys. Rev. Lett.* **2010**, *105*, 136805.
[2] T. Cao, G. Wang, W. Han, H. Ye, C. Zhu, J. Shi, Q. Niu, P. Tan, E. Wang, B. Liu, J. Feng, *Nat. Commun.* **2012**, *3*, 887.
[3] K. F. Mak, K. He, J. Shan, T. F. Heinz, *Nat. Nanotechnol.* **2012**, *7*, 494.
[4] H. Zeng, J. Dai, W. Yao, D. Xiao, X. Cui, *Nat. Nanotechnol.* **2012**, *7*, 490.
[5] A. Splendiani, L. Sun, Y. Zhang, T. Li, J. Kim, C. Y. Chim, G. Galli, F. Wang, *Nano Lett.* **2010**, *10*, 1271.
[6] G. Eda, H. Yamaguchi, D. Voiry, T. Fujita, M. Chen, M. Chhowalla, *Nano Lett.* **2011**, *11*, 5111.
[7] Y. Wang, C. Cong, C. Qiu, T. Yu, *Small* **2013**, *9*, 2857.
[8] X. Yin, Z. Ye, D. A. Chenet, Y. Ye, K. O'Brien, J. C. Hone, X. Zhang, *Science* **2014**, *344*, 488.
[9] H. S. Lee, S. W. Min, Y. G. Chang, M. K. Park, T. Nam, H. Kim, J. H. Kim, S. Ryu, S. Im, *Nano Lett.* **2012**, *12*, 3695.
[10] K. Roy, M. Padmanabhan, S. Goswami, T. P. Sai, G. Ramalingam, S. Raghavan, A. Ghosh, *Nat. Nanotechnol.* **2013**, *8*, 826.
[11] H. Xu, J. Wu, Q. Feng, N. Mao, C. Wang, J. Zhang, *Small* **2014**, *10*, 2300.
[12] J. Miao, W. Hu, Y. Jing, W. Luo, L. Liao, A. Pan, S. Wu, J. Cheng, X. Chen, W. Lu, *Small* **2015**, *11*, 2392.
[13] Y. H. Lee, X. Q. Zhang, W. Zhang, M. T. Chang, C. T. Lin, K. D. Chang, Y. C. Yu, J. T. Wang, C. S. Chang, L. J. Li, T. W. Lin, *Adv. Mater.* **2012**, *24*, 2320.
[14] S. Balendhran, J. Z. Ou, M. Bhaskaran, S. Sriram, S. Ippolito, Z. Vasic, E. Kats, S. Bhargava, S. Zhuiykov, K. Kalantar-Zadeh, *Nanoscale* **2012**, *4*, 461.
[15] A. M. van der Zande, P. Y Huang, D. A. Chenet, T. C. Berkelbach, Y. You, G. H. Lee, T. F. Heinz, D. R. Reichman, D. A. Muller, J. C. Hone, *Nat. Mater.* **2013**, *12*, 554.
[16] T. Ando, *J. Phys. Soc. Jpn.* **2006**, *75*, 074716.
[17] K. Dolui, I. Rungger, S. Sanvito, *Phys. Rev. B* **2013**, *87*, 165402.
[18] C. R. Dean, A. F. Young, I. Meric, C. Lee, L. Wang, S. Sorgenfrei, K. Watanabe, T. Taniguchi, P. Kim, K. L. Shepard, J. Hone, *Nat. Nanotechnol.* **2010**, *5*, 722.
[19] R. Gillen, J. Robertson, J. Maultzsch, *Phys. Rev. B* **2014**, *90*, 075437.
[20] X. Ling, Y. H. Lee, Y. Lin, W. Fang, L. Yu, M. S. Dresselhaus, J. Kong, *Nano Lett.* **2014**, *14*, 464.
[21] M. Buscema, G. A. Steele, H. S. J. van der Zant, A. Castellanos-Gomez, *Nano Res.* **2014**, *7*, 561.
[22] S. Wang, X. Wang, J. H. Warner, *ACS Nano* **2015**, *9*, 5246.
[23] P. Blake, E. W. Hill, A. H. Castro Neto, K. S. Novoselov, D. Jiang, R. Yang, T. J. Booth, A. K. Geim, *Appl. Phys. Lett.* **2007**, *91*, 063124.

[24] A. Castellanos-Gomez, N. Agraït, G. Rubio-Bollinger, *Appl. Phys. Lett.* **2010**, *96*, 213116.
[25] M. M. Benameur, B. Radisavljevic, J. S. Héron, S. Sahoo, H. Berger, A. Kis, *Nanotechnology* **2011**, *22*, 125706.
[26] J. A. Wilson, A. D. Yoffe, *Adv. Phys.* **1969**, *18*, 193.
[27] S.-L. Li, H. Miyazaki, H. Song, H. Kuramochi, S. Nakaharai, K. Tsukagoshi, *ACS Nano* **2012**, *6*, 7381.
[28] G. Plechinger, J. Mann, E. Preciado, D. Barroso, A. Nguyen, J. Eroms, C. Schüller, L. Bartels, T. Korn, *Semicond. Sci. Technol.* **2014**, *29*, 064008.
[29] B. Chakraborty, A. Bera, D. V. S. Muthu, S. Bhowmick, U. V. Waghmare, A. K. Sood, *Phys. Rev. B* **2012**, *85*, 161403.
[30] C. Liu, Y. Ma, W. Li, L. Dai, *Appl. Phys. Lett.* **2013**, *103*, 213103.
[31] E. Franke, M. Schubert, J.-D. Hecht, H. Neumann, T. E. Tiwald, D. W. Thompson, H. Yao, J. A. Woollam, J. Hahn, *J. Appl. Phys.* **1998**, *84*, 526.
[32] H. Zhang, Y. Ma, Y. Wan, X. Rong, Z. Xie, W. Wang, L. Dai, *Sci. Rep.* **2015**, *5*, 8440.
[33] K. F. Mak, K. He, C. Lee, G. H. Lee, J. Hone, T. F. Heinz, J. Shan, *Nat. Mater.* **2013**, *12*, 207.

Received: July 19, 2015
Revised: September 27, 2015
Published online: November 25, 2015

